Electrochemically Top Gated Graphene: Monitoring Dopants by Raman Scattering

A. Das[1], S. Pisana[2], S. Piscanec[2], B. Chakraborty[1], S. K. Saha[1], U. V. Waghmare[3], R.Yiang[4], H.R.Krishnamurhthy[1], A. K. Geim[4], A. C. Ferrari[2],* and A.K. Sood[1†]

[1] *Department of Physics, Indian Institute of Science, Bangalore 560012,India*

[2] *Cambridge University, Engineering Department, 9 JJ Thomson Avenue, Cambridge CB3 OFA, UK*

[3] *TSU, Jawaharlal Nehru Centre for Advanced Scientific Research,Bangalore 560064, India*

[4] *Department of Physics and Astronomy, Manchester University,UK*

We demonstrate electrochemical top gating of graphene by using a solid polymer electrolyte. This allows to reach much higher electron and hole doping than standard back gating. In-situ Raman measurements monitor the doping. The G peak stiffens and sharpens for both electron and hole doping, while the 2D peak shows a different response to holes and electrons. Its position increases for hole doping, while it softens for high electron doping. The variation of G peak position is a signature of the non-adiabatic Kohn anomaly at Γ. On the other hand, for visible excitation, the variation of the 2D peak position is ruled by charge transfer. The intensity ratio of G and 2D peaks shows a strong dependence on doping, making it a sensitive parameter to monitor charges.

The recent discovery of thermodynamically stable two-dimensional single and few layers graphene[1,2,3,4] has led to many experimental and theoretical advances in two dimensional physics and devices[5]. In particular, near ballistic transport at room temperature and high carrier mobilities (between 3000 and 25000 cm^2/Vs)[2,3] make graphene a potential material for nanoelectronics[6,7,8].

Electrochemical top gating is key to enable polymer transistors[9,10]. It has also been successfully applied for nanotubes[11,12,13,14,15]. Here we demonstrate a top-gated graphene transistor able to span much higher doping levels than previously reported. Electron and hole doping up to $\sim 5\times10^{13}cm^{-2}$ is achieved by solid polymer electrolyte gating. Such a high doping level is possible because the nanometer thick Debye layer[12,13,16] gives a much higher gate capacitance compared to the commonly used 300 nm thick SiO_2 back gate[17]. A significant advantage of a solid polymer electrolyte over electrolytes in solution is that it does not degrade the sample and the electrodes, while the gate leakage current is negligible compared to the drain current[13]. Graphene's response to the polymer electrolyte also shows its potential for both electronic and molecular sensing.

Doping is monitored by in-situ Raman spectroscopy together with transport measurements. Raman spectroscopy is a powerful non-destructive technique to identify the number of layers, structure, doping and disorder[18,19,20,21]. The prominent Raman features in graphene are the G-band at Γ ($\sim$1584 cm^{-1}), and the 2D band at $\sim$ 2700 cm^{-1} involving phonons at $\mathbf{K}+\Delta\mathbf{k}$ points in the Brillouin zone[18,21]. The value of $\Delta\mathbf{k}$ depends on the excitation laser energy, due to a double-resonance Raman process and the linear dispersion of the phonons around K[18,22,23]. The effect of doping induced by SiO_2 back gating on the G-band frequency and full width at half maximum (FWHM) has been reported recently[19,20]. This results in G peak stiffening and linewidth decrease for both electron and hole doping. The decrease in linewidth saturates when doping causes a Fermi level shift bigger than half the phonon energy[19,20]. The strong electron-phonon coupling in graphene and metallic nanotubes gives rise to Kohn anomalies in the phonon dispersions[23,24,25], which result in phonon softening. The G peak stiffening is due to the non-adiabatic removal of the Kohn-anomaly from Γ[19]. The FWHM(G) sharpening happens because of the blockage of the decay channel of phonons into electron-hole pairs due to the Pauli exclusion principle, when the electron-hole gap becomes higher than the phonon energy[19,20,25,26,27,28]. A similar behavior is observed for the LO-G^- peak of doped metallic nanotubes[11,29], for exactly the same reasons.

In the previous Raman studies on doped graphene[19,20], a $\sim$300 nm SiO_2 gate was used. This limited the maximum doping levels to less than $1\times10^{13}cm^{-2}$. The maximum G peak upshift was less than 10 cm^{-1}. Here, we focus on the simultaneous evolution of the G and 2D peaks. The G peak stiffens and sharpens for both electron and hole doping. On the other hand, the 2D peak shows a different response to holes and electrons. Its position markedly increases for hole doping, while it softens for high electron doping. The intensity ratio of 2D and G shows a strong dependence on doping, making it a sensitive parameter to monitor Fermi level shifts.

Graphene samples are produced by micro-mechanical cleavage of bulk graphite and deposited on Si covered with 300 nm SiO_2 (IDB Technologies LTD)[17]. Raman spectroscopy is used to select single layers[18]. Source and drain Au electrodes are then deposited by photolithography as shown in Fig.1. Top gating is achieved by using solid polymer electrolyte consisting of $LiClO_4$ and polyethelyne oxide (PEO) in the ratio 0.12:1, as previously used for nanotubes[13]. The gate voltage is applied by placing a platinum electrode in the polymer layer[13,16]. Electrical measurements are done using Keithley 2400 source meters. Fig. 1 shows the schematic of the experimental setup for transport and Raman measurements. Raman spectra of pristine and back gated samples are measured with a Renishaw spectrometer. In-situ measurements on top gated graphene are recorded using a WITEC confocal (X50 objective) spectrometer with

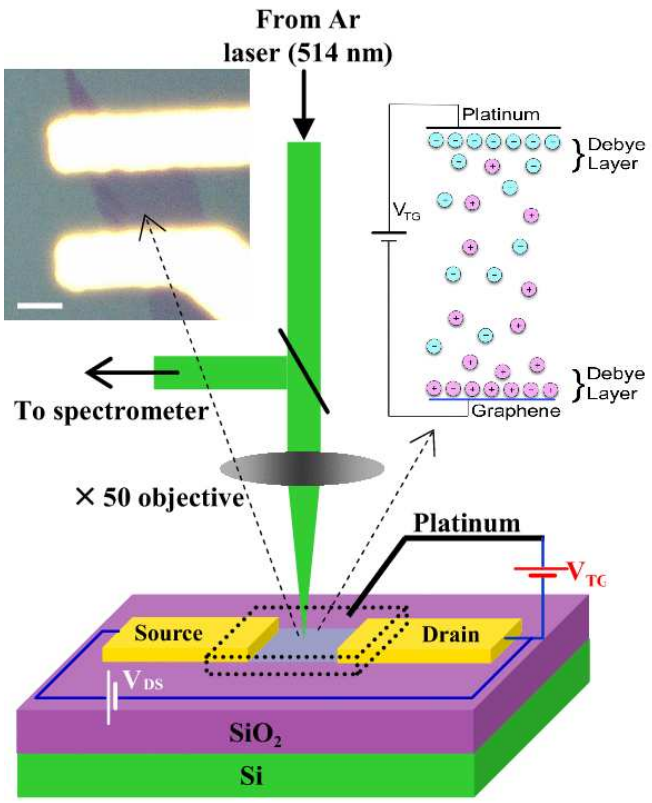

FIG. 1: (color online). Schematic diagram of the experimental setup. The black dotted box between the drain-source indicates the thin layer of polymer electrolyte (PEO + $LiClO_4$). The left inset shows the optical image of a single layer graphene connected between source and drain gold electrodes. Scale bar: 5μm. The right inset is a schematic illustration of polymer electrolyte top gating, with Li^+ and ClO_4^- ions and the Debye layers near each electrode.

600 lines/mm grating, 514.5 nm excitation and very low power level ($\sim$ 1mW) to avoid any heating effect. The spectral resolution of the two instruments is determined by fitting the Rayleigh line to a Gaussian profile and is 1.9 cm^{-1} for the Renishaw spectrometer and 9.4 cm^{-1} for WITEC spectrometer. The Raman spectra are then fitted with Voigt functions. The FWHM of the Lorentzian components give the relevant information on the phonon lifetime. Note that a very thin layer of polymer electrolyte does not absorb the incident laser light. Furthermore the Raman spectrum of the polymer does not cover the signatures of graphene, as will be discussed later. The measured source-drain currents (I_{SD}) and G, 2D peaks are reversible at different gate voltages. In transport experiments a small hysteresis in current ($\sim$1 μA) is observed during forward and backward gate voltage scans (at a intervals of 10 minutes for each gate voltage step). On the other hand, the Raman hysteresis $\leq$ 1 cm^{-1}.

We finally compare our experimental results with Density Functional Perturbation theory (DFPT) simulations[30]. Calculations are performed within the generalized gradient approximation (GGA)[31]. We use plane-waves (30 Ry cut-off) and pseudopotential [32] approaches. The semi-metallic character of the system is treated by performing the electronic integration with a Fermi-Dirac first-order spreading with a smearing of 0.01 Ry[33]. Integration over the BZ is done with an uniform $72 \times 72 \times 1$ k-points grid. Calculations are done using the Quantum Espresso code[34].

We first consider the electrical response. In order to compare our top gating results with back gating measurements, it is necessary to convert the top gate voltage into an effective doping concentration. In general, the application of a gate voltage (V_G) creates an electrostatic potential difference ϕ between graphene and the gate electrode and a Fermi level, E_F, shift as a result of addition of charge carriers. Therefore,

$$V_G = \frac{E_F}{e} + \phi \qquad (1)$$

ϕ and E_F/e are determined by the geometrical capacitance, C_G, and the chemical (quantum) capacitance of graphene, respectively.

Let us first consider back gating (BG). For a back gate, $\phi = \frac{ne}{C_{BG}}$ where n is the carrier concentration and C_{BG} is the geometrical capacitance. For single layer graphene $C_{BG} = \frac{\epsilon\epsilon_0}{d_{BG}}$, where ϵ is the dielectric constant of SiO_2 ($\sim$4), ϵ_0 is the permitivity of free space and d_{BG} is 300 nm. This results in a very low gate capacitance C_{BG} = 1.2×10^{-8}Fcm^{-2}. Therefore, for a typical value of n = 1×10^{13} cm^{-2}, the potential drop is ϕ = 100 V, much larger than $\frac{E_F}{e}$. Hence, $V_{BG} \approx \phi$ and the doping concentration becomes $n = \eta V_{BG}$, where $\eta = C_{BG}/e$. However, most samples have a zero-bias (V_{BG}=0) doping of, typically, a few 10^{11} cm^{-2}[21,17,35]. This is reflected in the existence of a finite gate voltage V_{nBG} at which the Hall resistance is zero and the longitudinal resistivity reaches its maximum. This maximum is associated with the Fermi level positioned between the valence and the conduction bands (the Dirac point). Accordingly, a positive (negative) V_{BG}-V_{nBG} induces electron (holes) doping, with an excess-electron surface-concentration of $n=\eta(V_{BG} - V_{nBG})$. A value of $\eta \approx 7.2\times10^{10}cm^{-2}V^{-1}$ is found from Hall effect measurements and agrees with the estimation from the gate geometry[1,2,3,4].

Let us consider the present case of top gating (TG). First we briefly discuss how the polymer electrolyte works as a gate. When a field is applied, free cations tend to accumulate near the negative electrode, creating a positive charge there and an uncompensated negative charge near the interface. The accumulation is limited by the concentration gradient, which opposes the Coulombic force of the electric field. When a steady state is reached, the statistical space charge distribution resembles that shown in Fig. 1. This layer of charge around an electrode is called the Debye layer. As shown in Fig. 1, when we apply a positive potential (V_{TG}) to the platinum top gate, with respect to the source electrode connected to graphene, the Li^+ ions become dominant in the Debye layer formed

at the interface between graphene and the electrolyte. The Debye layer of thickness d_{TG} acts like a parallel plate capacitor. Therefore, the geometrical capacitance in this case is $C_{TG} = \frac{\epsilon\epsilon_0}{d_{TG}}$, where ϵ is the dielectric constant of the PEO matrix. The Debye length is given by $d_{TG} = (2ce^2/\epsilon\epsilon_0 kT)^{-1/2}$ for a monovalent electrolyte where c is the concentration of the electrolyte, e is the electric charge, kT is the thermal energy[36]. In principle, d_{TG} can be calculated if the electrolyte concentration is known. However, in presence of a polymer, the electrolyte ions form complexes with the polymer chains[37,38]. Hence the exact concentration of ions is not amenable to measurement. For polymer electrolyte gating the Debye layer thickness is reported to be a few nanometers ($1 \sim 5$ nm)[13,39]. The dielectric constant (ϵ) of PEO is 5[40]. Assuming a Debye length of 2 nm, we get a gate capacitance $C_{TG} = 2.2\times 10^{-6}$ F cm^{-2}, which is much higher than C_{BG}. Therefore, the first term in equation (1) cannot be neglected. The Fermi energy in graphene changes as $E_F(n) = \hbar|v_F|\sqrt{\pi n}$, where $|v_F| = 1.1 \times 10^6 ms^{-1}$[2,3,20] is the Fermi velocity, hence:

$$V_{TG} = \frac{\hbar|v_F|\sqrt{\pi n}}{e} + \frac{ne}{C_{TG}} \qquad (2)$$

Using the values of C_{TG} and v_F,

$$V_{TG}(volts) = 1.16 \times 10^{-7}\sqrt{n} + 0.723 \times 10^{-13} n \qquad (3)$$

where n is in units of cm^{-2}. Eq. 3 allows us to estimate the doping concentration at each top gate voltage (V_{TG}). Note that, as in back gating, we also get the minimum source-drain current at finite top gate voltage ($V_{nTG} = 0.6$ V), as seen in Fig. 2a. Accordingly, a positive (negative) V_{TG}-V_{nTG} induces electron (holes) doping.

Fig. 2a shows the source-drain current (I_{SD}) of the top gated graphene as a function of electrochemical gate voltage. Note that for each point a given gate voltage is applied for 10 minutes to stabilize I_{SD}. The gate dependence of the drain current (Fig. 2a) shows ambipolar behavior and is almost symmetric for both electron and hole doping. This directly relates to the band structure of graphene, where both electron and hole conduction are accessible by shifting the Fermi level. The I_{SD}-V_{SD} characteristics at different electrochemical gate voltages (Fig. 2b) show linear behavior, indicating the lack of significant Schottky barriers at the electrode-graphene interface.

Fig. 3a plots the resistivity of our graphene layer (extracted from Fig. 2a knowing the sample's aspect ratio: W/L = 1.55) as a function V_{TG}. Fig.3b shows the back gate response of the same sample (without electrolyte). There is an increase in resistivity maximum (~ 6 kΩ) after pouring the electrolyte, which may originate from the creation of more charged impurities on the sample. Fig. 3 also shows that for both TG and BG experiments the resistivity does not decay sharply around the Dirac point. Indeed, it has been suggested that the sharpness of the resistivity around the Dirac point and the finite offset gate voltage (V_{nBG}) depend on charged impurities[17,41,42].

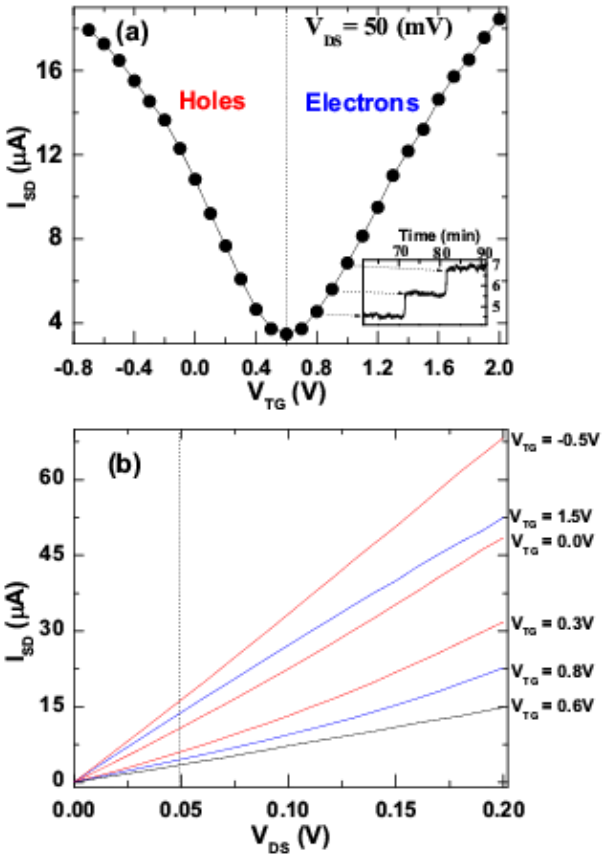

FIG. 2: (color online). (a) I_{SD} as a function of top gate voltages (V_{TG}). The inset shows the I_{SD} time dependence at fixed V_{TG}. The dotted line corresponds to the Dirac point. (b) I_{SD} vs V_{DS} at different top gate voltages. Red and blue lines correspond to hole and electron doping, respectively. The black dotted line corresponds to the source-drain value at which the gate dependence curve is measured.

The conductivity minimum (σ_{min}) (resistivity maximum) is obtained when the Fermi level is at the Dirac point. This is generally around $\sim 4\frac{e^2}{h}$[2,17]. In both our back and top gate experiments the conductivity minimum is reduced by the contact resistance, since measurements are performed in the two-probe configuration. As the contact resistance is expected to depend strongly on the carrier concentration (due to formation of a p-n junction around the contact and changing in the density of states in graphene) we can only give an estimation of the lower bound of the contact resistance. As shown in Fig. 3a, the resistivity saturates at ~ 4.2 kΩ (which corresponds to a 2.7 kΩ resistance) when the carrier density in the sample is the highest. Therefore, we estimate our contact resistance to be around 2.7 kΩ. Subtracting the effect of contact resistance, the minimum conductivity in our sample is $\sim 1.3\frac{e^2}{h}$. Minimum conductivities in the range from $2\frac{e^2}{h}$ to $10\frac{e^2}{h}$ were recently reported[41], with the spread assigned to charged impurities.

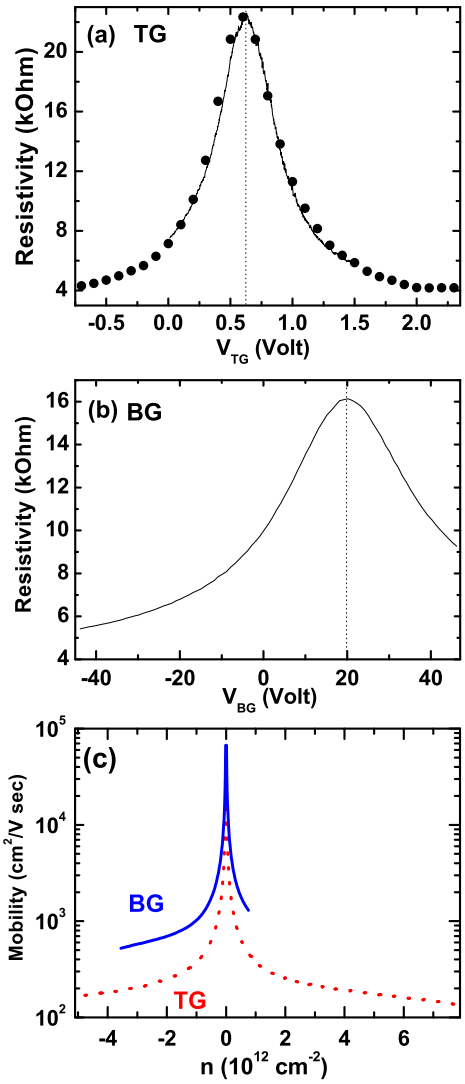

FIG. 3: (Color online).(a) Resistivity as a function of top gate. The dots are extracted from Fig.2a for W/L = 1.55. The solid line corresponds to the resistivity change as a function of V_{TG}, where the gate voltage is varied at a intervals of 2mV. (b) Resistivity of the same sample as a function of back gate. The dotted black line marks the Dirac point. (c) Mobility as function of doping for TG (red dotted) and (BG) (solid blue).

Fig.3c shows the change in mobility (using the simple Drude model $\mu = (en\rho)^{-1}$[41]) as a function of doping for our TG/BG experiments. The mobility is smaller in the TG case. This is consistent with the reduction in conductivity minimum and can be attributed to the presence of added charge impurities from the polymer electrolyte. Despite the limitations in 'on' and 'off' currents, our large graphene device shows an on/off ratio of ~ 5.5. This is higher than what previously reported for devices using 20 nm thick SiO_2 as top gate (on/off ratio ~ 1.5)[6] and 40 nm thick PMMA as a top gate (on/off ratio ~ 2)[43].

We now consider the evolution of the Raman spectra. Fig. 4a,b plot the Raman spectra for $V_{BG} = 0$ V and

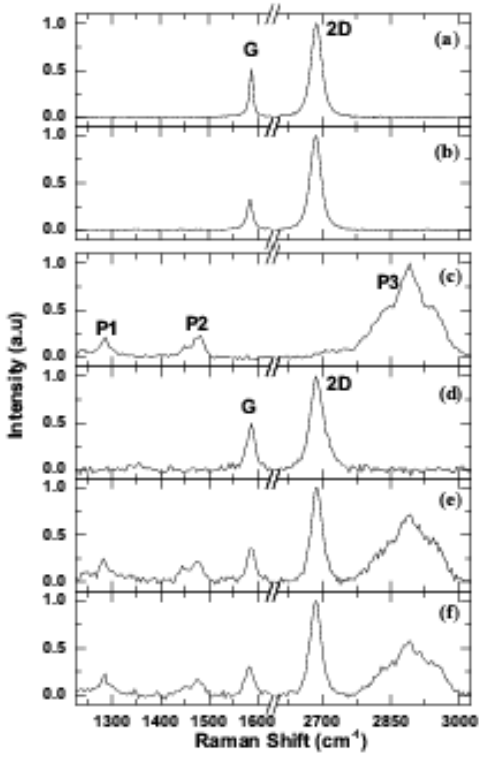

FIG. 4: Raman spectra at (a) $V_{BG} = 0.0$ V and (b) V_{BG}=V_{nBG}=20V. (c) Raman spectra of PEO+$LiClO_4$ mixture. (d) Raman spectra of graphene before pouring the polymer electrolyte. (e) Raman spectra at $V_{TG} = 0.0$ V and (f) V_{TG}=V_{nTG}=0.6V. P1, P2 and P3 are the polymer peaks[44]

$V_{nBG} = 20$ V. Fig. 4c to 4f show the spectra recorded during the top gate experiment. Fig. 4c is the PEO Raman spectrum. This has three prominent peaks at ~ 1282 cm^{-1} (P1), 1476 cm^{-1} (P2) and 2890 cm^{-1} (P3), which correspond to twisting, bending and stretching modes of the CH_2 bonds in the polymer[44]. Luckily they do not overlap the main features of graphene (see Figs. 4d,f). Furthermore these PEO Raman lines do not change with gating. Table 1 shows the comparison of G peak position, Pos(G), FWHM(G) and 2D/G height ratio, I(2D)/I(G), at zero gate voltage and the Dirac point for BG and TG.

TABLE I: G peak position, FWHM and 2D/G height ratio.

Gate Voltage	Pos(G) (cm^{-1})	FWHM(G) (cm^{-1})	I(2D)/I(G) (height ratio)
$V_{BG} = 0.0$ V	1586.7	8.7	2.0
$V_{nBG} = 20$ V	1584.0	12.6	3.1
$V_{TG} = 0.0$ V	1586.4	13.9	2.75
$V_{nTG} = 0.6$ V	1583.1	14.9	3.3

Table 1 shows that at the Dirac point (V_{nBG} and V_{nTG}) we have the lowest Pos(G), maximum FWHM(G)

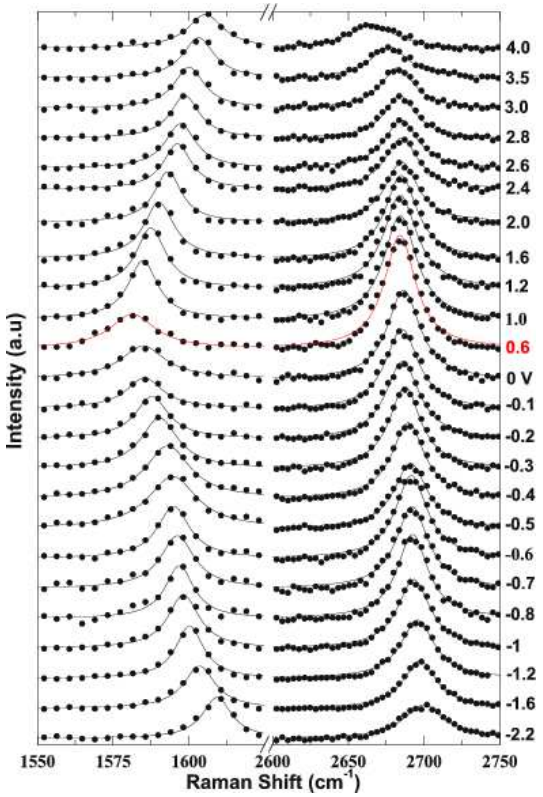

FIG. 5: (Color online). Raman spectra at several V_{TG}. The dots are the experimental data. Black lines are fitted Lorentzians. The red line corresponds to the Dirac point.

and I(2D)/I(G). However, our sample has a lower I(2D)/I(G), FWHM(G) and higher Pos(G) than the most intrinsic samples measured to date[18,35], due to the presence of charge impurities[35].

Fig.5 plots the Raman spectra as a function of top gate voltages. Fig. 6,7 show the Raman parameters as a function of doping. The minimum Pos(G) ($\sim$ 1583.1 cm^{-1}) is at $V_{TG} = V_{nTG} \sim 0.6$ V. Pos(G) increases for positive (V_{TG} - V_{nTG}) and negative (V_{TG} - V_{nTG}), i.e. for both electron and hole doping, by up to 30 cm^{-1} for hole doping and 25 cm^{-1} for electron doping (see Fig. 6a). The decrease in FWHM(G) (see Fig. 6b) for both hole and electron doping is similar to earlier results[19,20], even though extended to a much wider doping range. Most interestingly, the 2D peak shows a very different dependence on gate voltages when compared to the G mode. For electron doping, Pos(2D) does not change much ($<$ 1 cm^{-1}) until gate voltage of $\sim$ 3V (corresponding to $\sim 3.2\times10^{13}$cm^{-2}). At higher gate voltages, there is a significant softening by $\sim$ 20 cm^{-1} and for hole doping, Pos(2D) increases by $\sim$ 20 cm^{-1} (see Fig. 7a).

Fig.8 plots the variation of G and 2D intensity ratio (I(2D)/I(G))as a function of doping. These show a strong dependence on doping. The dependence of the 2D mode is much stronger than that of the G mode and hence the 2D/G intensity ratio is a strong function of the gate voltage. Therefore, this ratio is an important

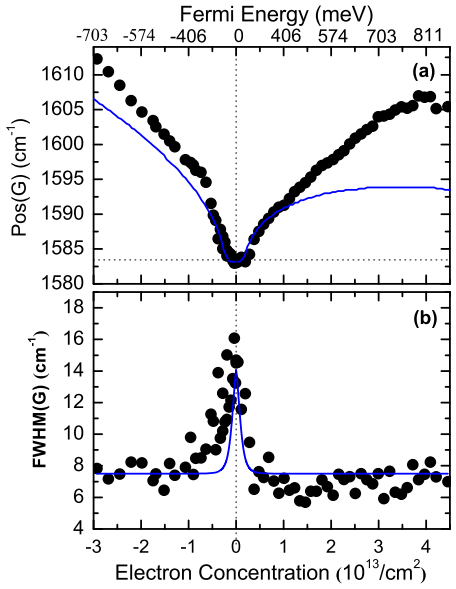

FIG. 6: (color online). (a) Pos(G) and (b) FWHM(G) as a function of electron and hole doping. The solid blue lines are the predicted non-adiabatic trends from Refs.[19,26].

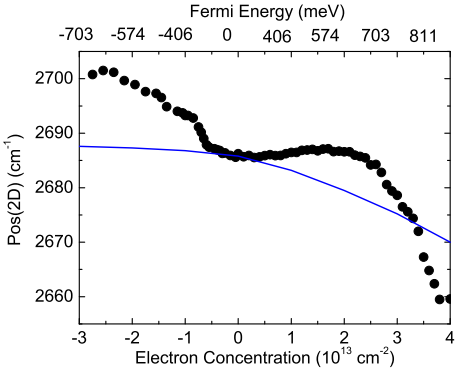

FIG. 7: (color online).(a) Pos(2D) as a function of doping. The solid line is our adiabatic DFT calculation.

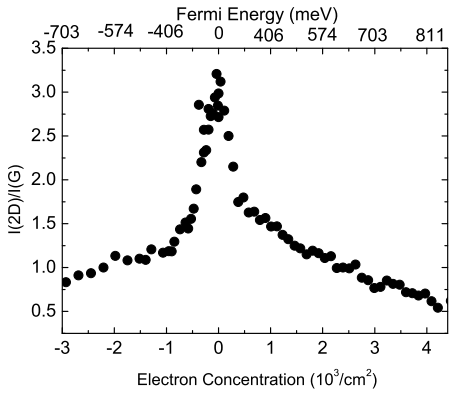

FIG. 8: I(2D)/I(G) as a function of hole and electron doping.

parameter to estimate the doping density. A similar dependence is expected for nanotubes. Figs.8,6 also show that I(2D)/I(G) and G peak position should not be used to estimate the number of graphene layers, unlike what suggested in refs.[45,46]. The shape of the 2D being the most effective way to identify a single layer[18].

The theoretical trends in Fig.6 were discussed before[19,26]. These confirm previous back gate experiments, but extend the data to a much wider electron and hole range[19]. In this wider range, the theory still captures the main features, such as the asymmetry between electrons and hole doping[26], however the quantitative agreement is poor for large doping, and requires to reconsider the non-adiabatic calculations of Ref.[26].

Here we focus on the novel trend of 2D peak position as a function of doping. *This is experimentally and conceptually different from the G peak.*

The 2D peak is due to second order, double resonant (DR) Raman scattering[18,22,47]. In this process, the incoming laser radiation creates an electron-hole pair close to the Fermi point $\mathbf{k}_F = \mathbf{K}$. The photo-excited electron is then scattered towards the second inequivalent Fermi point $\mathbf{k}_F = \mathbf{K}'$ by a phonon of energy $\hbar\omega_q$ and wavevector $\mathbf{q}$. A scattering event with a second phonon, of the same energy but opposite momentum, brings the electron back to its original position in reciprocal space. The recombination of the electron-hole couple finally results in the emission of a photon, whose energy is decreased by $2\hbar\omega_{\mathbf{q}}$ with respect to the incoming laser radiation. The order of these four events is not fixed, and all their combinations are possible and have to be taken into account[47].

The position of the 2D-peak can be evaluated by computing the energy of the phonon involved in the second-order, double resonant scattering process. As shown in Ref.[18], due to the trigonal warping of the $\pi - \pi^*$ bands and the angular dependence of the electron-phonon coupling (EPC), only phonons oriented along the **ΓKM** direction and with $\mathbf{q} > \mathbf{K}$ give a non-negligible contribution to the 2D-peak. The precise value of q is fixed by the constraint that the energy of the incoming photons $\hbar\omega_L$ has to exactly match a real electronic transition. In particular only a wavevector $\mathbf{q}'$ can be found for which $\hbar\omega_L = \epsilon(\pi^*, \mathbf{q}') - \epsilon(\pi, \mathbf{q}')$, where $\epsilon(n, \mathbf{k})$ is the energy of an electron of band index n and wavevector $\mathbf{k}$, and $\mathbf{q}'$ is measured from $\mathbf{K}$ and is in the **ΓKM** direction. Once $\mathbf{q}'$ has been determined, $q = 2q' + K$. Among the six phonons corresponding to the $\mathbf{q}$ vector that satisfy the DR conditions, only the highest optical branch has an energy compatible to the measured Raman shift. Therefore, the theoretical position of the 2D peak corresponds to twice the energy of the Raman active phonon.

In order to compare with our experiments performed at 514nm, we consider $\hbar\omega_L = 2.5$ eV. Assuming the π/π^* bands to be linear, with a slope of 14.1 eV[23], this laser energy selects a phonon with wavevector $\mathbf{q}$ of modulus 0.844 in $\frac{2\pi}{a_0}$ units, a_0 being the lattice parameter of graphene. The dependence of Pos(2D) on doping can be investigated by calculating, within a DFT framework, the effects of the Fermi level shift on the phonon frequencies.

In doped graphene, the Fermi energy shift induced by doping gives two major effects: (i) a change of the equilibrium lattice parameter with a consequent stiffening/softening of the phonons, and (ii) the onset of effects beyond the Adiabatic Born-Oppenheimer approximation that modify the phonons close to the Kohn anomalies[19,26]. The excess (defect) charge gives an expansion (contraction) of the crystal lattice. This was extensively investigated to understand graphite intercalation compounds[48]. We model the Fermi surface shift by varying the number of electrons in the system. Since the total energy of charged systems diverges, electrical neutrality is achieved by imposing a uniformly charged background. To avoid electrostatic interactions between graphene and the background, the equilibrium lattice parameter of the charged system is computed in the limit of a infinite volume unit cell. Such limit is reached using a model with periodic boundary conditions where the graphene layers are spaced by 60 Å. Phonon calculations for charged graphene are done using the same unit cells employed for the determination of the corresponding lattice parameter. Interestingly, while we observe that for charged graphene the frequency of zone boundary TO phonons converge only for layer spacing as large as 60 Å, the frequency of the E_{2g} mode is already converged for a 7.5 Å spacing.

Dynamic effects beyond Born-Oppenheimer play a fundamental role in the description of the KA in single wall carbon nanotubes and in graphene[19,24,26]. However, for the 2D peak measured at 514nm the influence of dynamic effects is expected to be negligible, since the phonons giving rise to the 2D-peak are far away from the Kohn anomaly at $\mathbf{K}$. Thus, we can calculate the position of the 2D-peak without dynamic corrections.

The comparison between the theoretical and the experimental position of the 2D peak is shown in Fig. 7a by a solid line. Our calculations are in qualitative agreement with experiments, considering the spectral resolution and the Debye layer estimation. Indeed, as experimentally determined, the position of the 2D peak is predicted to decrease for an increasing electron concentration in the system. This allows to use the 2D peak to discriminate between electron and hole doping.

The trade-off between measured and theoretical data can be partially explained in terms of the electrostatic difference existing between the experiments and the model DFT system. In our simulations the 2D phonon frequencies are very sensitive to the charged background used to ensure global electrical neutrality. In the experiments the electric charge on the graphene surface is induced by capacitative coupling. The electrostatic interaction between graphene and the electrolyte could thus further modify the 2D phonons. This does not affect the G peak to the same extent, due to the much lower sensitivity the G phonon to an external electrostatic potential.

In conclusion, we have demonstrated graphene top gating using a solid polymer electrolyte. We reached much

higher electron and hole doping than standard SiO_2 back gating. The conductivity minimum and mobility are reduced due to presence of charges. The Raman measurements show that the G and 2D peaks have different doping dependence and the 2D/G height ratio changes significantly with doping, making Raman an ideal tool for graphene nanoelectronics.

We thank K. S. Novoselov for useful discussions. AKS thanks the Department of Science and Technology, India for the financial support. SP acknowledges funding from Pembroke College and the Maudslay Society. ACF from the Royal Society and Leverhulme Trust.

* Electronic address: acf26@eng.cam.ac.uk
† Electronic address: asood@physics.iisc.ernet.in

[1] Novoselov, K. S.; Geim, A. K.; Morozov, S. V.; jiang, D.; Zhang, Y.; Dubonos, S. V.; Grigorieva, I. V.; Firsov, A. A. *Science* **2004**,*306*, 666.
[2] Novoselov, K. S.; Geim, A. K.; Morozov, S. V.; jiang, D.; Katsnelson, M. I.; Grigorieva, I. V.; Dubonos, S. V.; Firov, A. A. *Nature* **2005**, *438*, 197.
[3] Zhang, Y.; Tan, Y. -W.; Stormer, H. L.; Kim, P. *Nature* **2005**, *438*, 201.
[4] Novoselov, K. S.; Jiang, D.; Schedin, F.; Booth, T. J.; Khotkevich, V. V.; Morozov, S. V.; Geim, A. K. *PNAS* **2005**, *102*, 10451.
[5] Novoselov, K. S.; jiang, Z.; Morozov, S. V.; Stomer, H. L.; Zeitler, U.; Maan, J. C.; Boebinger, G. S.; Kim, P.; Geim, A. K. *Science* **2007**, *315*, 1379.
[6] Lemme, M.C.; Echtermeyer, T.J.; Baus, M.; Kurz, H. *IEEE Electr. Device Lett* **2007**, *28*, 282.
[7] Han, M. Y.; Ozyilmaz, B.; Zhang, Y.; Kim, P. *Phys. Rev. Lett.* **2007**, *98*, 206805.
[8] Chen, Z.; Lin, Y. M.; Rooks, M. J.; Avouris, P. *cond-mat/0701599* **2007**.
[9] Sirringhaus, H.; Kawase, T.; Friend, R. H.; Shimonda, T.; Inbasekaran, M.; Wu, W.; Woo, E. P. *Science* **2000**, *209*, 2123.
[10] Dhoot, A. S.; Yuen, J. D.; Heeney, M.; McCulloch, I.; Moses, D.; Heeger, A. J. *PNAS* **2006**, *103*, 11834.
[11] Nguyen, K. T.; Gaur, A.; Shim, M. *Phys. Rev. Lett.* **2007**, *98*, 145504.
[12] Ozel, T.; Gaur, A.; Rogers, J. A.; Shim, M. *Nano. Lett.* **2005**, *5*, 905.
[13] Lu, C.; Fu, Q.; Huang, S.; Liu, J. *Nano Lett.* **2004**, *4*, 623.
[14] Kruger, M.; Buitelaar, M. R.; Nussbaumer, T.; Schonenberger, C.; Forro, L. *Appl. Phys. Lett.* **2001**, *78*, 1291.
[15] Rosenblatt, S.; Yaish, Y.; Park, J.; Gore, J.; Sazonova, V.; McEuen, P. L. *Nano Lett.* **2002**, *2*, 869.
[16] Siddons, G. P.; Merchin, D.; Back, J.H.; Jeong, J. K; Shim, M. *Nano Lett.* **2004**, *4*, 927.
[17] Geim, A.K.; Novoselov, K.S., *Nature Materials* **2007**, *6*, 183.
[18] Ferrari, A. C.; Meyer, J. C.; Scardaci, V.; Casiraghi, C.; Lazzeri, M.; Mauri, F.; Piscanec, S.; Jiang, Da.; Novoselov, K. S.; Roth, S.; Geim, A.K. *Phys. Rev. Lett.* **2006**, *97*, 187401.
[19] Pisana, S.; Lazzeri, M.; Casiraghi, C.; Novoselov, K.; Geim, A. K.; Ferrari, A. C.; Mauri, F. *Nature Materials* **2007**, *6*, 198.
[20] Yan, J.; Zhang, Y.; Kim, P.; Pinczuk, A. *Phys. Rev. Lett.* **2007**, *98*, 166802.
[21] Ferrari, A. C. *Solid State Comm.* **2007**, *143*, 47.
[22] Thomsen, C.; Reich, S. *Phys. Rev. Lett.* **2000**, *85*, 5214.
[23] Piscanec, S.; Lazzeri, M.; Mauri, F.; Ferrari, A.; Robertson, J. *Phys. Rev. Lett.* **2004**, *93*, 185503.
[24] Piscanec, S.; Lazzeri, M.; Robertson, J.; Ferrari, A. C.; Mauri, F. *Phys. Rev. B* **2007**, *75*, 035427.
[25] Lazzeri, M.; Piscanec, S.; Mauri, F.; Ferrari, A. C.; Robertson, J. *Phys. Rev. B* **2006**, *73*, 155426.
[26] Lazzeri, M.; Mauri, F. *Phys. Rev. Lett.* **2006**, *97*, 266407.
[27] Ando, T. *J. Phys. Soc. Jpn.* **2006**, *75*, 124701.
[28] Castro Neto, A. H.; Guinea, F. *Phys. Rev. B* **2007**, *75*, 045404.
[29] Wu, Y.; Maultzsch, J.; Knoesel, E.; Chandra, B.; Huang, M.; Sfeir, M. Y.; Brus, L. E.; Hone, J.; Heinz, T. F. Phys. Rev. Lett. **99**, 027402 (2007).
[30] Baroni, S.; De Gironcoli, S.; Dal Corso, A.; Giannozzi, P. *Rev. Mod. Phys.* **2001**, *73*, 515.
[31] Perdew, P.; Burke, K.; Ernzerhof, M. *Phys. Rev. Lett.* **1996**, *77*, 3865.
[32] Troullier, N.; Martins, J. L. *Phys. Rev. B* **1991**, *43*, 1993.
[33] Methfessel, BM.; Paxton, A. T. *Phys. Rev. B* **1989**, *40*, 3616.
[34] www.quantum-esprsso.org.
[35] Casiraghi, C.; Pisana, S.; Piscanec, S.; Novoselov, K. S.; Geim, A. K.; Ferrari, A. C. submitted (2007)
[36] Tadmor, Rafael; Herna´ndez-Zapata, Ernesto; Chen, Nianhuan; Pincus, Philip; Israelachvili, Jacob N. *Macromolecules* **2002**, *35*, 2380.
[37] Frech, Roger; Chintapalli, Sangramithra; Bruce, Peter G.; Vincent, Colin A. *Macromolecules* **1999**, *32*, 808.
[38] Salomon, Mark; Xu, Meizhen; Eyring, Edward M.; Petrucci, Sergio *J. Phys. Chem.* **1994**, *98*, 8234.
[39] Donley, James P.; Rudnick, Joseph; Liu, Andrea J. *Macromolecules* **1997**, *30*, 1188.
[40] Boyd, Richard H. *journal*J. Polym. Sci. Polym. Phys. Ed **1983**, *21*, 505.
[41] Tan, Y. -W.; Zhang, Y.; Bolotin, K.; Zhao, Y.; Adam, S.; Hwang, E. H.; Sarma, S. Das; Stormer, H. L.; Kim, P. *cond-mat/0707.1807* **2007**.
[42] Adam, Shaffique; Hwang, E. H.; Galitski, V. M.; Sarma, S. Das *cond-mat/0705.1540* **2007**.
[43] Huard, B.; Sulpizio, J. A.; Stander, N.; Todd, K.; Yang, B.; Goldhaber-Gordon, D. Phys. Rev. Lett **98**, 236803 (2007).
[44] Yoshihara, Toshio; Tadokoro, Hiroyuki; Murahashi, Shunsuke *J. Chem. Phys.* **1964**, *41* 2902.
[45] Gupta, A.; Chen, G.; Joshi, P.; Tadigadapa, S.; Eklund, P. C., *Nano Lett.* **2006**, *6*, 2667.
[46] Graf, D.; Molitor, F.; Ensslin, K.; Stampfer, C.; Jungen, A.; Hierold, C.; Wirtz, L. *Nano Lett.* **2007**, *7*, 238.
[47] Maultzsch, J.; Reich, S.; Thomsen, C., *Phys. Rev. B* **2001**, *61*, 121407.
[48] Pietronero, L.; Strassler, S. *Phys. Rev. Lett.* **1981**, *47*, 593.